Nanotechnology Perceptions
ISSN 1660-6795
www.nano-*ntp.com*

Characterization And Antibacterial Evaluation Of Benzocaine-Derived Schiff Base Metal Complexes

Reena Bhatt[1]*, Shweta Mishra[1], and Niharika Shivhare[2]

[1]*Shri Vaishnav Vidyapeeth Vishwavidyalaya, Indore (M.P.) India.*
[2]*Prestige Institute of Management and Research, Indore (M.P.) India.*

Schiff bases are compounds containing the azomethine (-HC=N-) group, formed by the condensation of aldehydes or ketones with primary amines. These compounds serve as versatile ligands in the formation of transition metal complexes, which play a crucial role in developing new metal-based antibacterial agents and metal nanoparticles. Transition metal (II) complexes with Schiff base ligands exhibit significantly higher antibacterial activity than the free ligand, making them promising candidates for combating resistant bacterial strains. These complexes enhance biological activity by interacting with bacterial membranes and disrupting cellular functions. Additionally, Schiff base-metal complexes are widely studied for their potential applications in drug development, catalysis, and material science. This paper explores Schiff base ligands, their transition metal complexes, and their antibacterial properties, emphasizing their growing importance in medicinal and industrial chemistry. Their ability to form stable, bioactive complexes makes them valuable in modern therapeutic and antimicrobial research.

1.0 Introduction

Schiff bases, first identified by Hugo Schiff in 1864, are compounds featuring a C=N (imine) bond, formed through the condensation of aldehydes or ketones with primary amines. These compounds play a significant role in biological and chemical processes, particularly in metal complex formation, which enhances their antibacterial, antifungal, antitumor, and anti-inflammatory properties. Transition metals, located in groups 3–12 of the periodic table, possess partially filled d orbitals, multiple oxidation states, and strong catalytic abilities, making them ideal for forming stable Schiff base complexes. These complexes, particularly with metals like copper, cobalt, and zinc, exhibit notable biological activities, including potential applications in cancer treatment due to their interaction with DNA and selective cytotoxicity toward cancer cells. The advent of nanotechnology has further expanded the applications of Schiff base-metal complexes, as nanoparticles (≤100 nm) possess unique physical and chemical properties that make them suitable for targeted drug delivery and biomedical applications. Notably, Schiff base-metal complexes, especially those involving Fe(III), Co(II), Ni(II), and Cu(II), demonstrate significant antibacterial activity by disrupting bacterial cell walls and enhancing membrane permeability, offering promising solutions against resistant bacterial strains [1-8].

2.0 Methodology

2.1 Synthesis of Compound A

Compound A was synthesized by condensation reaction of acetyl acetone and o-toluiedine in alcoholic medium.

The preparation of Compound A takes place in following steps:

Step 1: Mixture of Acetyl acetone (0.01M) + Sodium acetate (0.01M) + 25 ml ethanol is refrigerated at 0 – 5 ◦C for few hours.
Step 2: Mixture of ortho toludine (0.01) + 10 ml HCl + 10 ml distilled water is kept in ice bath.
Step 3: Paste of Sodium nitrite (0.01) in minimum distilled water is kept in ice bath.
Step 4: Mixture in step 2 and paste of sodium nitrite in step 3 are mixed with constant stirring.
Step 5: The mixture obtained in step 4 is then added to the refrigerated mixture in step 1.

2.2 Synthesis of Compound B

This compound A was then treated with benzocaine to obtain Compound B. This reaction also proceeds in alcoholic medium.

2.3 Synthesis of Compound C

The compound B thus obtained is treated with metal (II) ions to get different complexes. The different metals used are Ni (II), Co (II) and Cu (II). The metal complexes synthesized are Compound C.

2.4 Characterization of Physical Properties [3, 9, 10]

1. Molecular Formula Determination:
    - Combines empirical formula analysis, molecular mass calculations, spectroscopic data, and refinement to deduce the compound's formula.
2. Molecular Weight Determination:
    - Summing atomic masses in the compound's formula provides the molecular weight in g/mol.
3. Melting Point Determination:
    - Uses controlled heating to observe the temperature range where the compound transitions from solid to liquid, indicating purity and identity.
4. Percentage Yield Calculation:
    - Compares actual product yield from a reaction to the theoretical maximum, expressed as a percentage:
      Percentage Yield=(Actual Yield/Theoretical Yield)×100%

2.5 UV/VIS Spectroscopy [3, 9, 10]

UV/VIS spectroscopy is an analytical technique that measures light absorption in the ultraviolet (UV), visible (VIS), and near-infrared (near-IR) regions. It provides insights into a substance's identity, structure, and concentration based on its unique absorption spectrum.

Measurement Process

A UV/VIS spectrophotometer compares light intensity before and after passing through a sample. It consists of:

- Light source
- Cuvette (sample holder)
- Monochromator (isolates specific wavelengths)
- Detector (measures transmitted light)

Absorbance is calculated by comparing the transmitted intensity of the sample to a solvent-only blank.

Transmittance and Absorbance

- Transmittance (T): Ratio of transmitted to initial intensity ($T = I/I0$)
- Absorbance (A): $A = -\log(T)$, correlating linearly with analyte concentration.

2.6 IR Spectroscopy [3, 9, 10]

IR spectroscopy analyzes molecular vibrations when exposed to infrared radiation. It covers Near IR (NIRS), Mid IR (MIRS), and Far IR (FIRS), studying fundamental vibrations, lattice vibrations, and metal-ligand interactions.

Principles

- Interaction with Molecules: IR radiation causes molecular vibrational state changes.
- Key Equations:
  - $c = \lambda\nu$ (speed of light, wavelength, frequency)
  - $E = h\nu$ (energy-frequency relationship)

Instrumentation

- Classical Dispersive Spectroscopy: Uses prisms/diffraction gratings.
- FT-IR Spectroscopy: Uses a Michelson interferometer for faster, higher resolution analysis.

2.7 X-ray Diffraction (XRD) [11-13]

XRD is a non-destructive method to study crystalline structures, identifying phases, crystallinity, grain size, and strain. It relies on X-ray scattering and Bragg's law.

Principles

- X-ray Generation: Produced by bombarding metal targets.
- Crystal Lattice & Diffraction: X-rays scatter based on atomic arrangements.
- Bragg's Law: $n\lambda = 2d \sin\theta$ (relates diffraction angle and interplanar spacing).

Instrumentation

- X-ray Source: Produces monochromatic X-rays.
- Sample Holder: Holds powder or single-crystal samples.
- Detector: Captures diffracted X-rays.
- Goniometer: Measures diffraction angles.

2.8 Scanning Electron Microscopy (SEM) [14, 15]

SEM is a high-resolution imaging technique for studying surface morphology, composition, and microstructures.

Principles

- Electron Beam Interaction: Generates secondary electrons (SEs), backscattered electrons (BSEs), and X-rays.
- Image Formation: Contrast results from surface topography and composition differences.

Instrumentation

- Electron Gun: Produces an electron beam.
- Electromagnetic Lenses: Focus the beam.
- Sample Chamber: Requires a vacuum environment.
- Detectors:
  - SE Detector: Captures surface details.
  - BSE Detector: Provides compositional contrast.
  - EDS: Performs elemental analysis.
- Vacuum System: Maintains low pressure.

2.9 Antimicrobial Resistance (AMR) [16-19]

AMR is a growing threat due to multidrug-resistant bacteria. Natural and synthetic antimicrobials, including nanoparticles, are being explored to combat resistance.

Sources of Antimicrobials

- **Natural**:
  1. Plants: Phytochemicals, alkaloids, saponins.
  2. Animals: Defensins, lysozymes.
  3. Microbes: Antibiotics, bacteriocins.
- **Synthetic**: Quinolones, triclosan, silver and zinc nanoparticles.

Screening Techniques

Agar Diffusion-Based Assays

- Methodology:
  1. Spread test microorganism on agar.
  2. Apply test substance in wells/discs.
  3. Incubate and measure inhibition zones.

- Advantages: Simple, cost-effective, standardized.
- Disadvantages: Primarily qualitative, diffusion variability.

3.0 Results and Discussion

3.1 Physical properties of the synthesised compounds

The physical properties for the ligand and the metal complexes synthesized are shown in table 1 below:

Table 1: The analytical data for the ligand and the metal complexes are shown in table below

Sr. No.	Compound		Molecular formula	Compound Name	Molecular weight	Colour	Melting point (◦C)	Yield (%)
1	A		$C_{12}H_{14}N_2O_2$	3-(2-O-tolylhydrazono)pentane-2,4-dione	218	Yellow	109	76
2	B		$C_{30}H_{32}N_4O_4$	(3-(2-O-tolylhydrazono)pentane-2,4-dione) benzoate	512	Yellow	107	72
3	C-Ni complex	Bulk	$C_{32}H_{40}N_4O_5NiCl$	(3-(2-O-tolylhydrazono)pentane-2,4-dione) benzoate Ni-complex	654.5	Light green	104	71
		Nano				Greenish	105	72
4	C-Cu complex	Bulk	$C_{32}H_{40}N_4O_5CuCl$	(3-(2-O-tolylhydrazono)pentane-2,4-dione) benzoate Cu-complex	659.0	Blueish	108	69
		Nano				Blueish	108	68
5	C-Zn complex	Bulk	$C_{32}H_{40}N_4O_5ZnCl$	(3-(2-O-tolylhydrazono)pentane-2,4-dione) benzoate Zn-complex	661.0	Light yellow	103	66
		Nano				Yellowish	105	68
6	C-Co complex	Bulk	$C_{32}H_{40}N_4O_5CoCl$	(3-(2-O-tolylhydrazono)pentane-2,4-dione) benzoate Co-complex	654.5	Light yellow	106	73
		Nano				Yellowish	108	72
7	C-Fe complex	Bulk	$C_{32}H_{40}N_4O_5FeCl$	(3-(2-O-tolylhydrazono)pentane-2,4-dione) benzoate Fe-complex	651.5	Light yellow	105	65
		Nano				Yellowish	105	68

The table presents the physical properties of the ligand and the synthesized metal complexes (both bulk and nano forms), including molecular formula, compound name, molecular weight, color, melting point, and percentage yield. Notably, the nano metal complexes generally exhibit a slightly higher yield compared to their bulk counterparts. The overall percentage yield for all metal complexes falls within the range of 65–72%.

3.2 FTIR Analysis

The FTIR spectra of the metal complexes, compared to those of the ligands, reveal a shift in the υ(C=N) band from 1629 cm^{-1} to a lower frequency by approximately 10–20 cm^{-1}, indicating coordination of the ligands to the metal ions through the nitrogen atom. Key absorption bands include υ(N-H) at 2240 cm^{-1}, υ(N=C) at 1629 cm^{-1}, υ(NC(Me)) at 2998 cm^{-1}, and υ(NC(Ar)) at 2120 cm^{-1}. Additionally, new bands observed exclusively in the metal complexes at 512 cm^{-1} and 519 cm^{-1} correspond to nitrogen-metal stretching vibrations. These findings confirm that the Schiff base ligand acts as a bidentate ligand. A comparison between experimental and theoretical data shows strong agreement, validating the accuracy and reliability of the theoretical results.

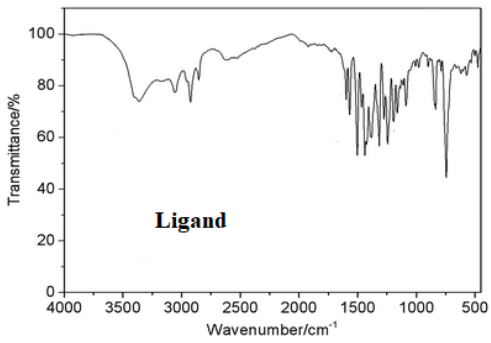

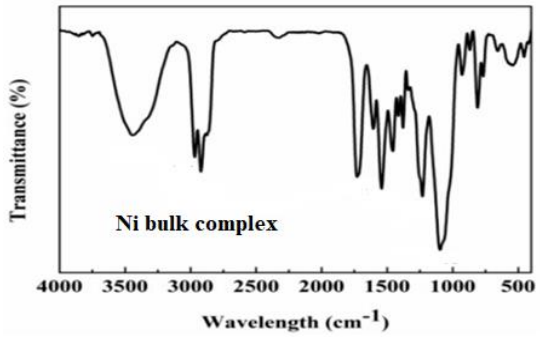

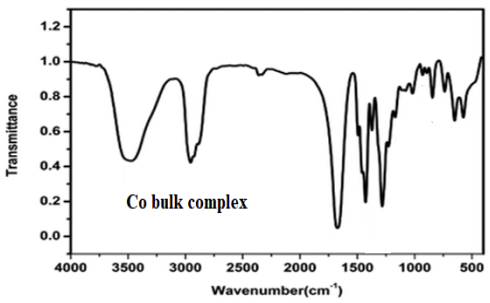

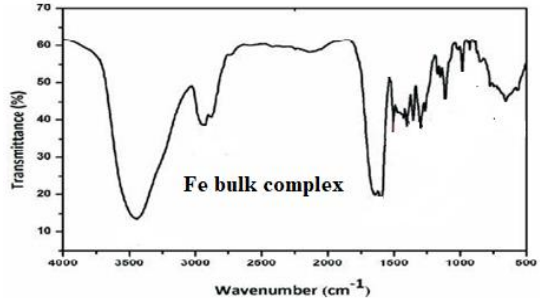

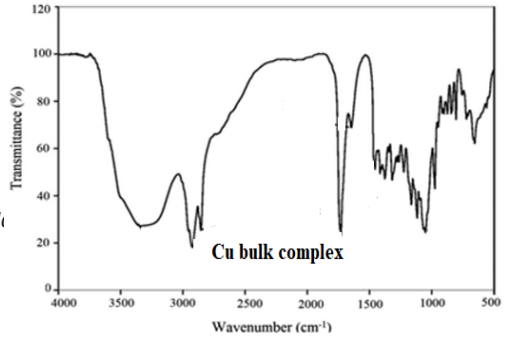

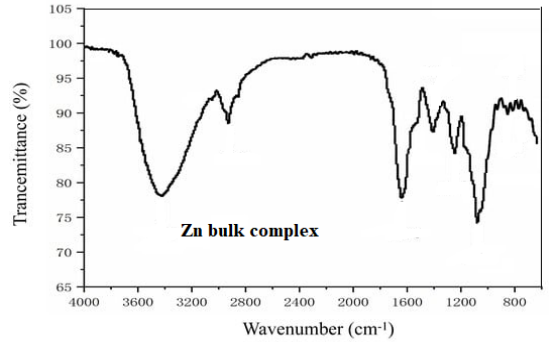

Figure 1: FTIR analysis for Compound C (bulk)

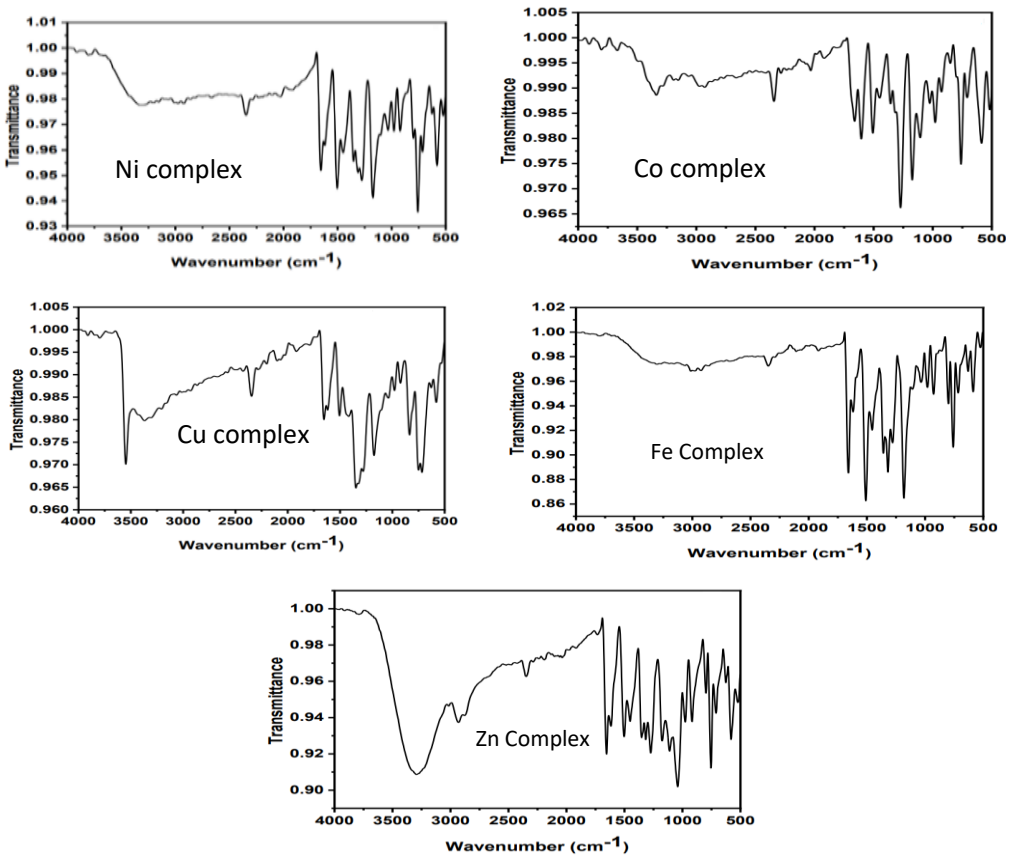

Figure 3: FTIR analysis for Compound C (nano)

3.3 XRD Analysis

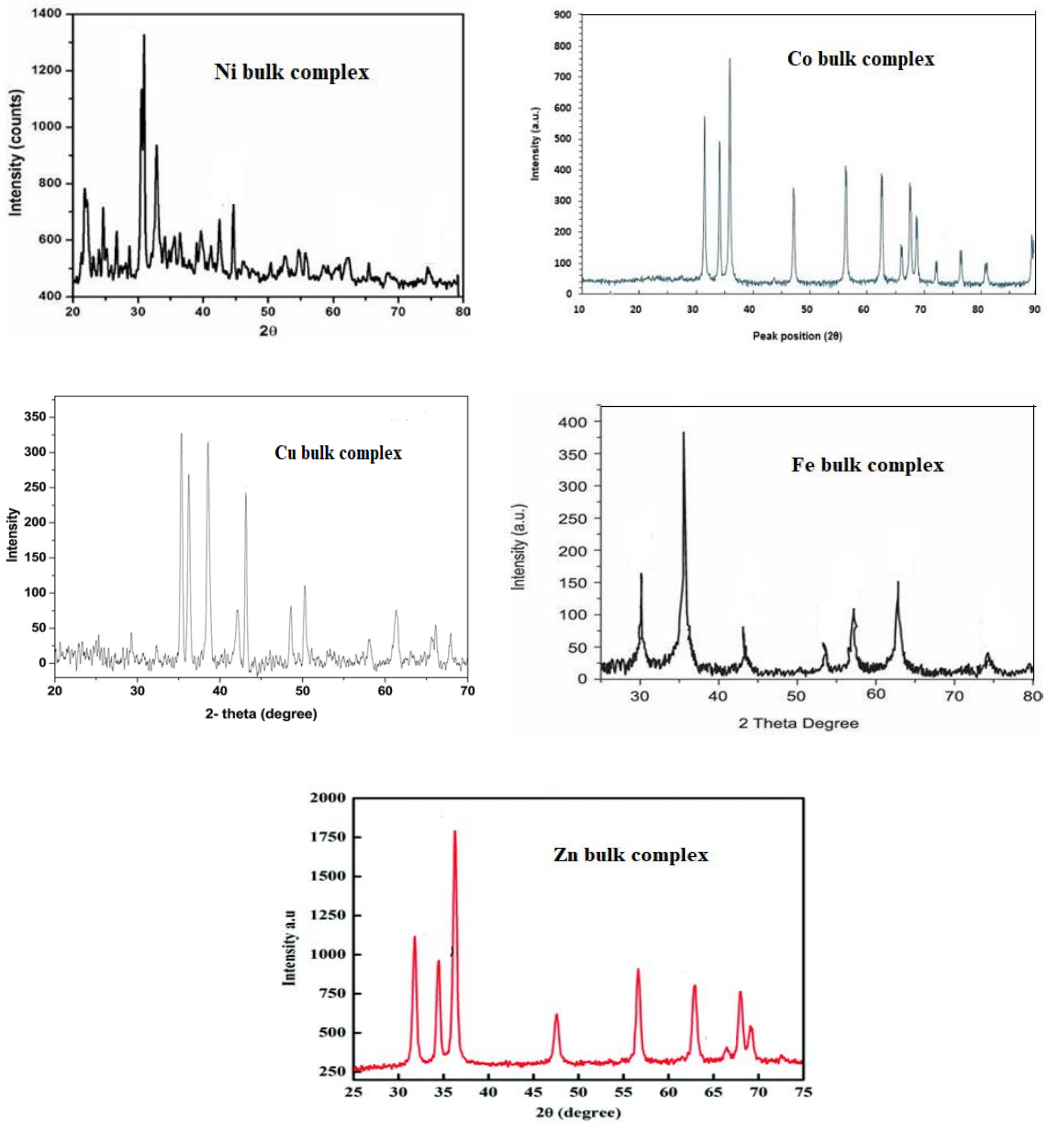

Figure 4: XRD for Compound C

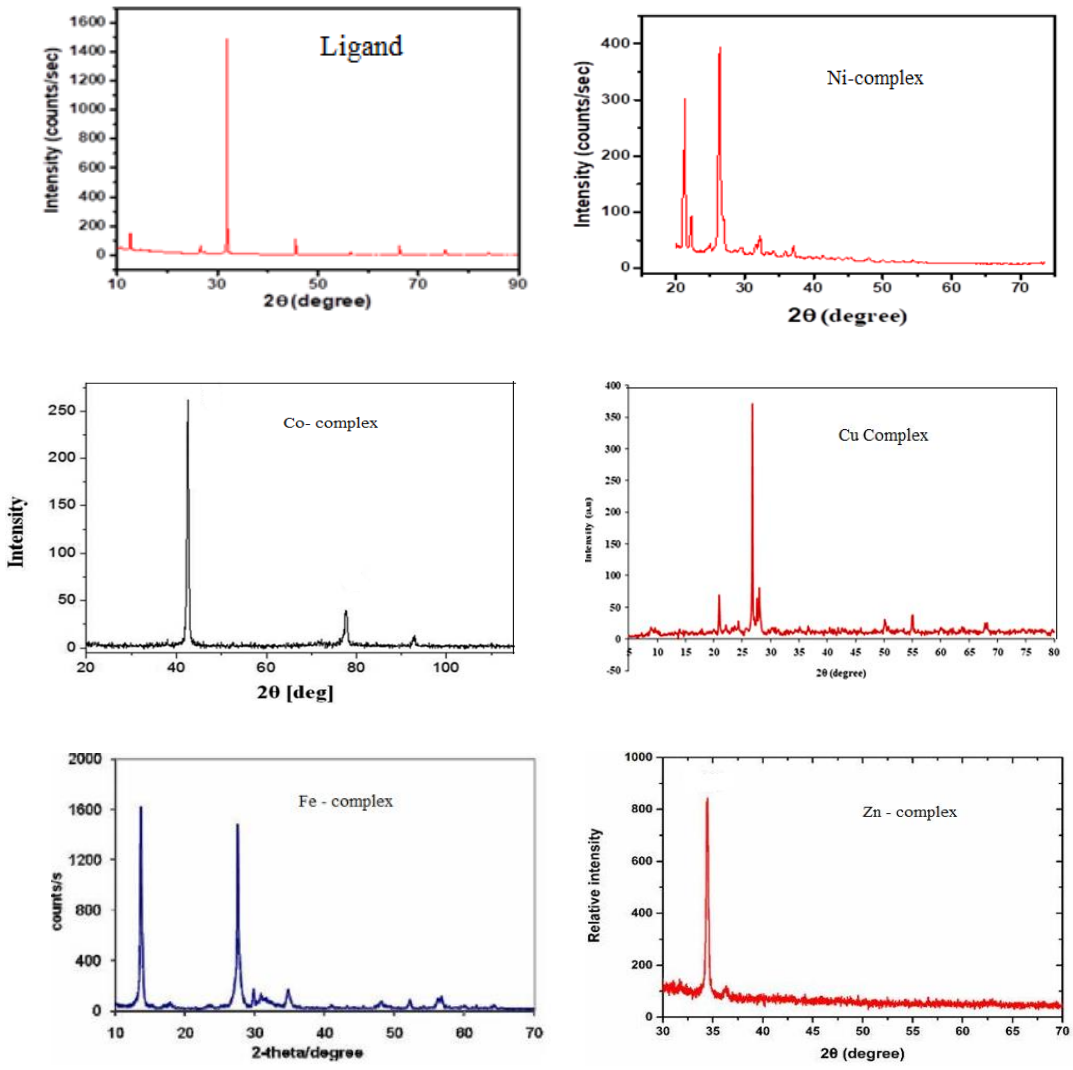

Figure 5: XRD for Compound B and C (nano)

Powder X-ray diffraction (PXRD) analysis was conducted to determine the crystalline size and structure of the synthesized Schiff base ligand and its metal complexes. The obtained X-ray diffraction patterns, as shown in the graphs, reveal the semi-crystalline nature of the metal complexes, confirmed by the presence of sharp and well-defined Bragg peaks at specific 2θ angles. The particle size of the complexes was estimated using the Debye-Scherrer formula, based on the intensity of the most prominent diffraction peak relative to the other peaks.

$D = 0.94 \lambda/\beta \cos \theta$
where, λ is the wavelength of the X-ray used, D is the crystalline size in nm, 0.94 is the sheerer constant,
β is the full width at half maximum (fwhm) and
θ is the position of the particular diffraction peak.

Table 2: The physical properties for the ligand and the metal complexes (bulk and nano)

Compound	Texture	Geometry	Crystal Quality	Crystalline size (D in nm)		Crystal distortion
				Bulk	Nano	
B	Crystalline	--	Good	48 ± 10		No
C- Ni complex	Crystalline	Octahedral	Good	52 ± 10	32 ± 10	No
C- Co complex	Crystalline	Octahedral	Good	55 ± 12	30 ± 10	No
C- Cu complex	Crystalline	Octahedral	Good	61 ± 14	35 ± 12	No
C- Fe complex	Crystalline	Octahedral	Good	58 ± 11	30 ± 11	No
C- Zn complex	Crystalline	Octahedral	Good	60 ± 11	36 ± 12	No

From the graphs above in figure 4-5 and table 2 it can be clearly seen that the nano metal complexes synthesized are crystalline and have good yield with octahedral geometry. The calculation of the inter planer spacing is also in the accordance of the good quality crystalline product obtained.

3.4 SEM Analysis

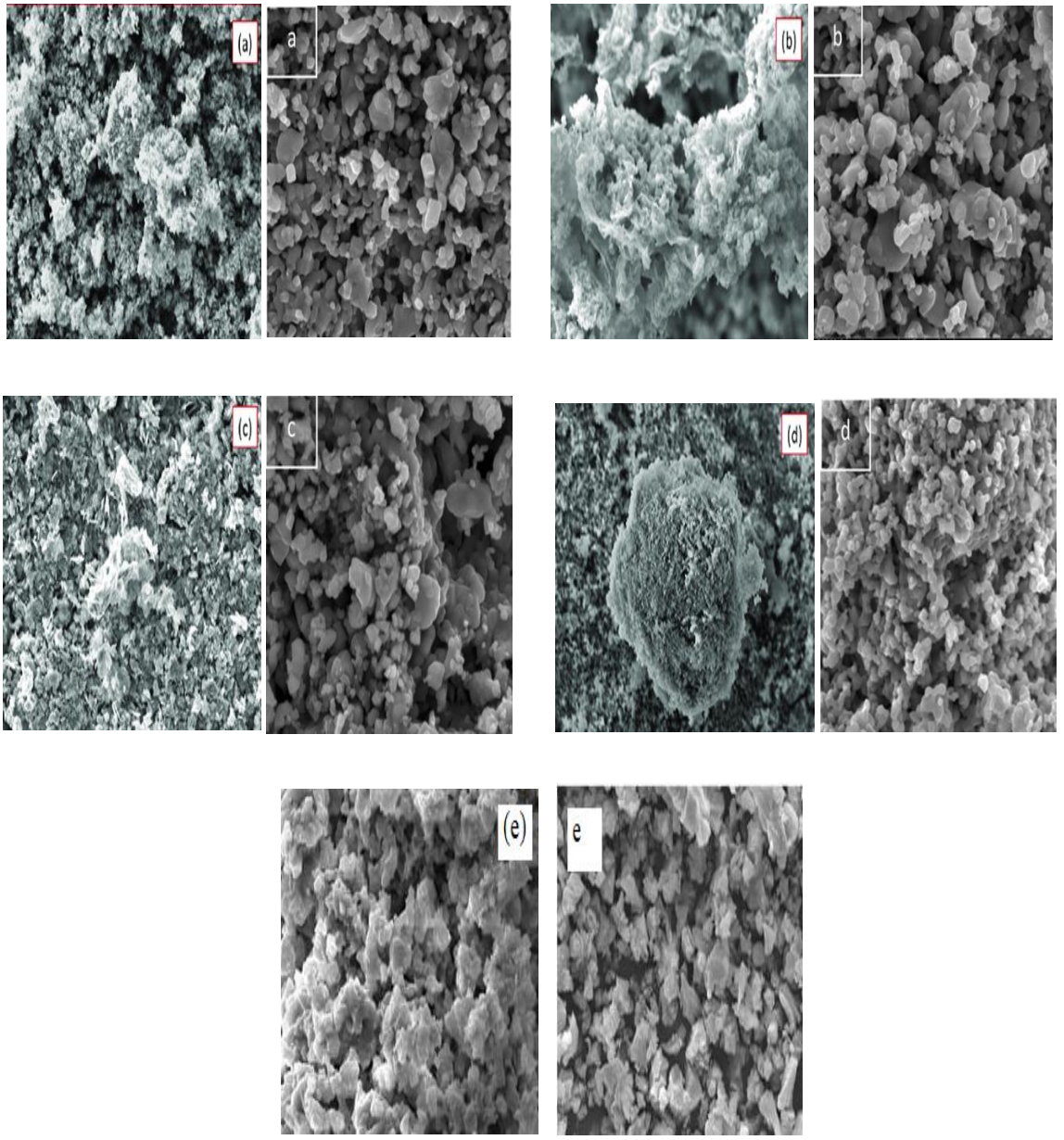

Figure 6: SEM images for Bulk synthesized and nano synthesized Compound C

a) Ni-Complex b) Cu-Complex c) Zn-Complex
d) Cu-Complex e) Fe-Complex

Scanning electron microscopy (SEM) was utilized to examine the micromorphology of the synthesized bulk and nano particles. SEM analysis provides crucial insights into the structural arrangement, density, and geometric features of materials in the solid state. The morphological differences between bulk and nano particles are evident, with nanoparticle morphology being influenced by the structure of the complexes. This analysis focuses on particle size, shape, and texture. The SEM images of the bulk and nano particles, presented in the previous figure, reveal distinct surface characteristics. The metal complexes of Co, Ni, Cu, and Zn exhibit semi-circular, flake-like, and needle-like shapes, respectively. The SEM images, measured in nanometers or micrometers, are shown in Figure 6.

3.5 Antibacterial Analysis

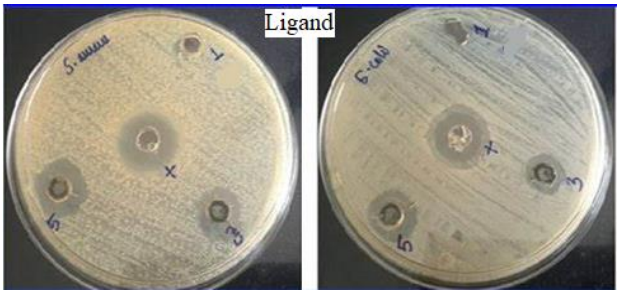

(a)

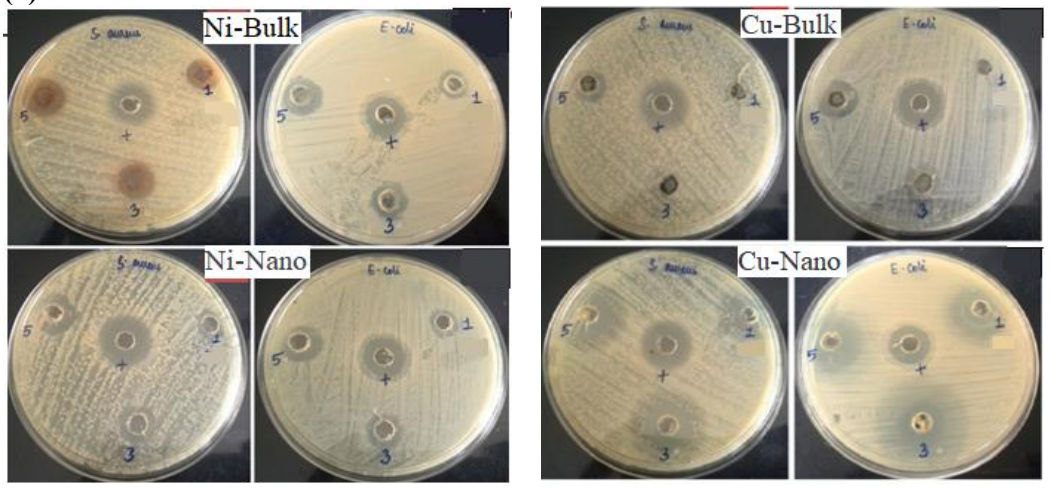

(b) **(c)**

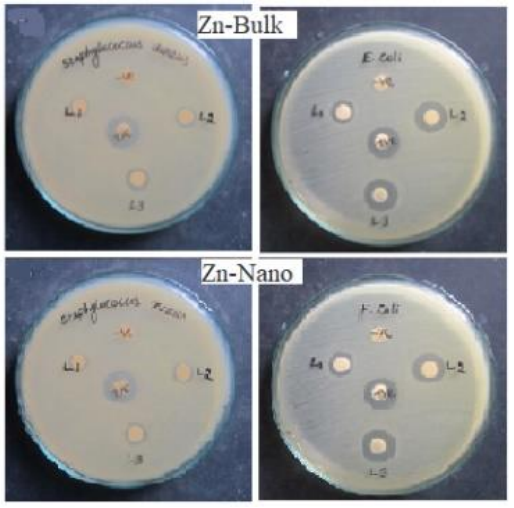

(d)

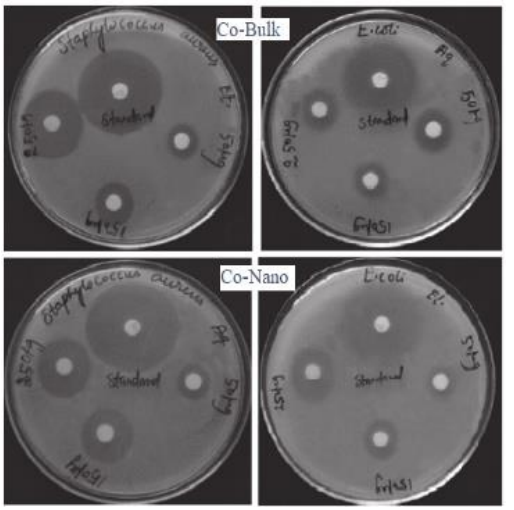

(e)

Figure 7: Antibacterial activity of S.aureus and E.coli against the ligand (a) and differently synthesized
Metal complexes (b) Ni-complex, (c) Cu-complex, (d) Zn-complex and (e) Co-complex

The antibacterial activity of Schiff base ligands and their soluble metal (II) complexes was evaluated against Staphylococcus aureus and Escherichia coli. The enhanced antibacterial activity of metal chelates can be explained by chelation theory, which suggests that chelation increases the ligand's potency, making the complexes more effective bacterial agents. In these complexes, the metal's positive charge is partially shared with donor atoms in the ligand, leading to π-electron delocalization across the chelate ring.

The antibacterial activity was assessed using the well diffusion method at two concentrations (100 and 200 µg/mL). In E. coli, higher concentrations (200 µg/mL) of the free ligand and metal complexes exhibited significant inhibitory effects. The Schiff base metal complexes of Co, Ni, Cu, Fe, and Zn were effective against E. coli and demonstrated good activity against S. aureus at a lower concentration (100 µg/mL). The results were compared to the standard antibiotic ciprofloxacin, revealing varying inhibition zone diameters.

Table 3: Antibacterial activity against gram +ve and gram –ve bacteria at different dosages

Parameter	Dosage		Ligand	Cu-Complex	Co-Complex	Zn-Complex	Ni-Complex
Zone of Inhibition (in mm)	For gram +ve bacteria Staphylococcus aureus						
	Bulk	100 µg/mL	15.1	15.3	14.8	13.8	8.0
		150 µg/mL	15.4	15.6	15.4	14.0	8.2
		200 µg/mL	16.3	15.7	15.8	14.6	8.3

	Nano	100 µg/mL	--	15.1	14.6	13.2	8.1
		150 µg/mL	--	15.6	15.8	14.2	8.2
		200 µg/mL	--	15.9	15.7	14.6	8.5
	For gram -ve bacteria Escherichia coli						
	Bulk	100 µg/mL	15.8	15.8	8.0	19.7	8.0
		150 µg/mL	15.5	15.5	8.1	18.8	8.0
		200 µg/mL	14.8	15.0	8.0	18.4	7.8
	Nano	100 µg/mL	--	15.7	8.2	19.3	8.1
		150 µg/mL	--	15.7	8.1	18.5	8.0
		200 µg/mL	--	14.8	8.0	18.1	8.2

The antibacterial activity of the metal complexes against Escherichia coli (gram-negative bacterium) follows the order:

Cu-Complex > Ligand > Co-Complex > Zn-Complex
Cu(II) and Co(II) complexes exhibit high antibacterial activity against E. coli, while the Zn(II) complex shows moderate activity.

For Staphylococcus aureus (gram-positive bacterium), the order of activity is:
Zn-Complex > Cu-Complex = Ligand > Co-Complex > Ni-Complex
Zn(II) and Cu(II) complexes are highly effective against S. aureus, whereas Co(II) and Ni(II) complexes show moderate activity. The bacterial activity images are presented in Figure.

Conclusion

A novel Schiff base ligand and its metal complexes were successfully synthesized via reflux reaction. Spectroscopic and analytical data support the octahedral geometry of all metal complexes. Nanoparticles were derived from these complexes through a decomposition process, and their morphology was confirmed using SEM analysis. Antibacterial screening revealed significant activity against pathogens. Theoretical studies further validate the bidentate coordination of the ligand through β-ketiminato functionality.

References

1. Xavier, N. Srividhya. IOSR Journal of Applied Chemistry 2014, 7(11), 06-15.
2. Shoaib K., Rehman W., Mohammad B., and Ali S., Journal of Proteomics & Bioinformatics, 2013, 6(7), 153–157.
3. Bhatt R., Mishra S. and Shivhare N. Synthesis, Nanotechnology Perceptions, 2024, 20(6), 977 – 987.
4. Vamsikrishna N., Daravath S., Ganji N., Pasha N., Inorg. Chem. Commun. 2020, 113, 107767.
5. Deodware S.A., Barache U.B., Chanshetti U.B., Sathe D., Ashok U.P., Gaikwad S.H., Kollur S.P., Resul. Chem. 2021, 3, 100162.
6. Yusuf T.L., Oladipo S.D., Zamisa S., Kumalo H.M., Lawal I.A., Lawal M.M., Mabuba N., ACS Omega, 2021, 6, 13704–13718.
7. Zhu J., Li X., Zhang S., Yan L., Spectrochim. Acta A Mol. Biomol. Spectrosc. 2021, 257, 119801.

8. Almehmadi M.A., Aljuhani A., Alraqa S.Y., Ali I., Rezki N., Aouad M.R., Hagar M., J. Mol. Struct. 2021, 1225, 129148.
9. Revathi N., Sankarganesh M., Dhaveethu Raja J., Vinoth Kumar G.G., Sakthivel A., Rajasekaran R., J. Biomol. Struct. Dyn. 2021, 39, 3012–3024.
10. Chandrasekar T., Arunadevi A., N. Raman, J. Coord. Chem. 2021, 74, 804–822.
11. Lee J-W, Park W B, Lee J H, et al. Nature Communications 2020 ; 11 : 86.
12. Ghanghas P., Choudhary A., Kumar D., Poonia K., Inorg. Chem. Commun. 2021, 130, 108710.
13. Rodriguez I, Gautam R, Tinoco A D. Biomimetics 2021; 6(1): 1.
14. Ma X., Zhou S., Xu X., Q.b Du, Front. Surg. 2022, 9, 905892.
15. Pathinathan U., Prabhakar S. Applied Surface Science Advances, 2023, 13, 100257.
16. Lima P.G., Oliveira J.T., Amaral J.L., Freitas C.D., Souza P.F., Life Sci. 2021, 278, 119647.
17. Silva da C., Silva da D., Modolo L., Alves R.: J. Ad. Res., 2011, 2, 1–8.
18. Yang X., Wang Q., Huang Y., Fu P., Zhang J., Zeng R. Inorg. Chem. Com., 2012, 25, 55–59.
19. Bocian A., Gorczynski A., D. Marcinkowski, S. Witomska, M. Kubicki, P. Mech, M. Bogunia, J. Brzeski, M. Makowski, P. Pawlu´c, J. Mol. Liq. 2020, 302, 112590.